



*Supplement of*

**Measurement report: The influence of particle number size distribution and hygroscopicity on the microphysical properties of cloud droplets at a mountain site**

**Xiaojing Shen et al.**

*Correspondence to:* Quan Liu (liuq@cma.gov.cn) and Junying Sun (jysun@cma.gov.cn)

The copyright of individual parts of the supplement might differ from the article licence.

The location of the observatory and cabinet

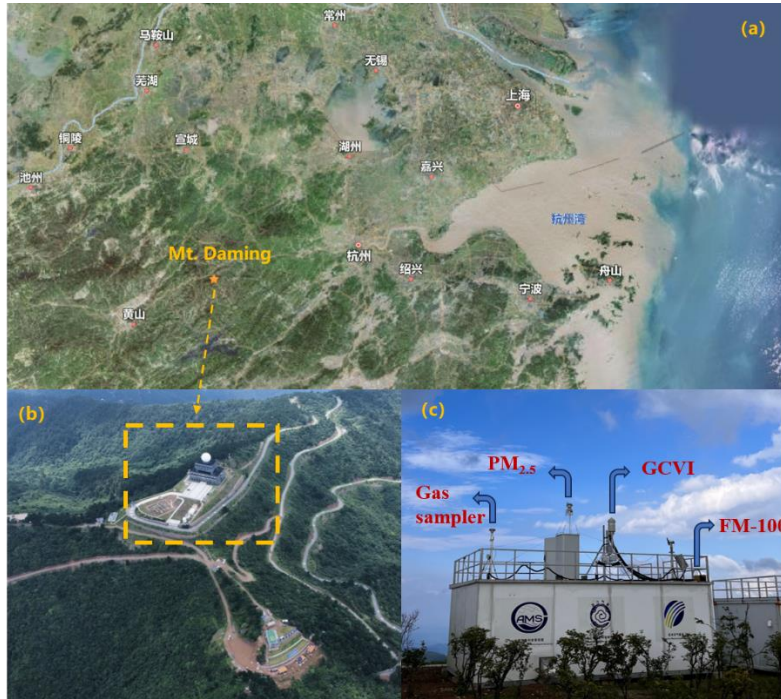


Fig. S1. The location of the observatory (a, b) and the experiment setup on the cabinet (c)

## Instrument calibration and data validation

### FM-100 and GCVI sampling efficiency correction

The GCVI sampling efficiency was corrected according to Karlsson et al., (2021), Pereira Freitas et al., (2024), Spiegel et al., 2012, and Shingler et al. (2012) as recommended. The slope of the linear regression (slope) and the  $R^2$  value (coefficient of determination) was 0.68 and 0.69, respectively. First, the fog monitor data was corrected based on the equation of  $\eta_{tot}(D_{pg}) = \eta_{smp}(D_{pg}) \times \eta_{tsp}(D_{pg})$  (Spiegel et al., 2012), where  $\eta_{tot}$ ,  $\eta_{smp}$ ,  $\eta_{tsp}$  is the total counting efficiency, sampling efficiency and transport efficient of the fog droplets with the size of  $D_{pg}$ .  $\eta_{smp}$  of fog particles with  $D_{pg} < 20 \mu\text{m}$  is approximate 1.0,  $\eta_{tsp}$  for particles  $< 10 \mu\text{m}$  is about 0.9-1.0 and for particles of 10-20  $\mu\text{m}$  is about 0.85-0.90. In our study, the fog droplets concentrated below 20  $\mu\text{m}$ , with the number concentration accounting for  $94 \pm 4.5\%$  to the total fog droplets. Thus, we only applied 0.95 for particles  $< 10 \mu\text{m}$  and 0.90 for 10-20  $\mu\text{m}$  droplets to correct the transport loss, and 1.0 for sampling loss. With this calculation, total counting efficiency for fog droplet data is 0.95. Second, the MCPC

data after GCVI inlet can be corrected by the corrected fog droplet size distribution multiplying by transmission efficiency experimentally determined by Shingler et al. (2012). Finally, the sampling efficiency of GCVI inlet can be derived based on the linear regression between the cloud residual particle number concentration (MCPC data) and the corrected cloud particles. In this work, the sampling efficiency was 0.68, and all the cloud residual particle number concentration and mass concentration have been revised. And the details of data correction have been supplemented in the supplementary material.

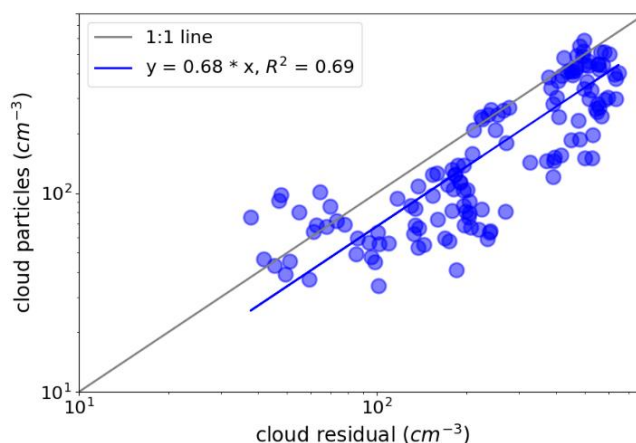


Fig. S2 The scatter plot of number concentration of cloud residual particle from MCPC of GCVI inlet and the corrected fog monitor data with GCVI sampling efficiency.

#### TSMPS calibration and data correction

About the TSMPS (TROPOS, Germany) applied in this work, we followed the calibration and data inversion routine as recommended by Wiedensohler et al., (2012). The size (PSL of 200 nm), sample flow and high voltage calibration was conducted before the start of this field campaign. The tube length and flow rate were also recorded to correct the diffusion loss. The multiple-charge correction and diffusion loss have been conducted by a custom-made data inversion software to make sure the accuracy of PNSD data.

The high voltage and size calibration was conducted for TSMPS before the measurement started. In the LabView software, we use multi-point calibration to ensure that the input and output voltages exhibit a linear ratio, with a slope of 1250. For example, we input a voltage of 20 mv, then we measure the output voltage, it should be

25 v, otherwise, we adjust the slope in the software and do the calibration again. We use Latex of 200 nm to do the size calibration, to make sure DMA select the accurate monodispersed aerosols. If the measured particle size deviates from the PSL by 3%, the sheath flow rate will need to be adjusted. When the HV and size calibration have been conducted, we should believe the PNSD data are almost accurate. The aerosol and sheath flow, as well as the zero check are conducted regularly once a week.

The diffusion loss was considered in the data inversion program, with the input of tube length and flow rate (Wiedensohler et al., 2012). Number concentration of particles below 100 nm ( $N_{<100\text{nm}}$ ) and above 100 nm ( $N_{\geq 100\text{nm}}$ ) are obtained by integrating PNSD. It shows  $N_{<100\text{nm}}$  with diffusion loss corrected is approximate 15% higher than the value without diffusion loss correction.  $N_{\geq 100\text{nm}}$  with diffusion loss corrected is approximate 2% higher, and almost no difference for particles above 200 nm (Fig. 3a). The difference between number concentration with diffusion loss corrected ( $N_{\text{diff,corr}}$ ) and without ( $N_{\text{no,diff,corr}}$ ) as indicated by the ratio of  $(N_{\text{diff,corr}} - N_{\text{no,diff,corr}}) / N_{\text{diff,corr}}$  shows significant size dependence.  $N_{\text{diff,corr}}$  can be 70% higher than  $N_{\text{no,diff,corr}}$  at 10 nm, and sharply decrease as the particle size increase (Fig. 3b). That means the diffusion loss can be ignored for particles above 100 nm. In this work, for the residual particles, which concentrate in the size above 100 nm, number concentration integrated from TSMPS ( $N_t$ ) better agreed with that from MCPC ( $N_{\text{mcpc}}$ ), with  $N_t$  being 9% higher. For CF and CR particles, which was dominated by the Aitken mode particles,  $N_t$  was 30-40% higher than  $N_{\text{mcps}}$ , because the diffusion loss correction was conducted for TSMPS, but not for MCPC. The difference was much large for CF particles, as new particle formation event sometimes occurred, and the diffusion loss could be larger.

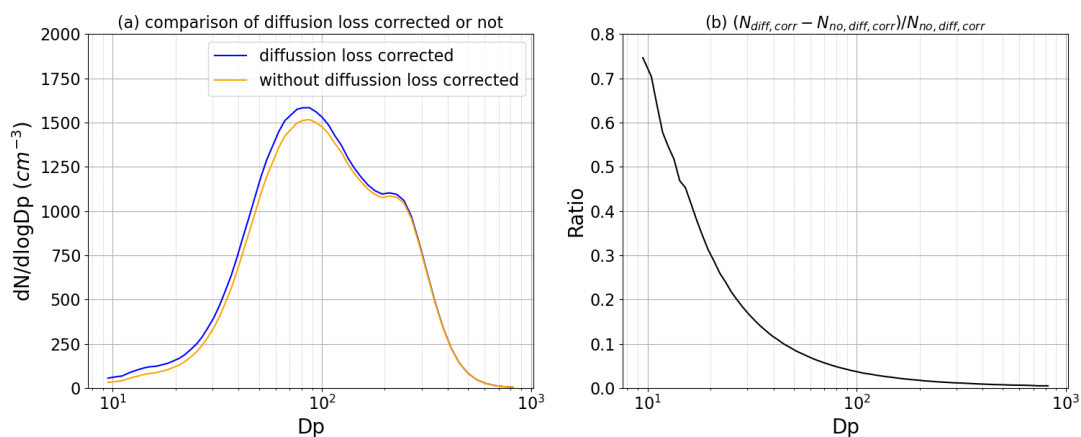


Fig.S3. The comparison between mean PNSD of a day (288 scans) with diffusion loss correction and not (a), and size dependent difference of particle number concentration with corrected diffusion loss ( $N_{\text{diff,corr}}$ ) and not  $N_{\text{no,diff,corr}}$

#### AMS calibration and data correction

The calibrations of ionization efficiency (IE) were performed, using size-selected (300 nm) ammonium nitrate particles before and after the experiment. Default relative IE values were used for organics (1.4), nitrate (1.1), sulfate (1.2), ammonium (4.0), and chloride (1.3), respectively. The HR-ToF-AMS collection efficiency (CE) accounts for the incomplete detection of aerosol species owing to particle bounce at the vaporizer, and/or the partial transmission of particles by the lens (Canagaratna et al., 2007). In this study, a composition-dependent CE correction was used, following the methodology described by Middlebrook et al. (2012). Positive matrix factorization (PMF) (Ulbrich et al., 2009) and a multilinear engine (ME-2) (Canonaco et al., 2013) modelling of high time resolution organic mass spectrometric data from HR-ToF-AMS have also been used to resolve organics into primary organic aerosols (POA) and oxygenated organic aerosols (OOAs), which correspond to different sources and processes (Zhang et al., 2022).

The mean PNSD and standard deviation for cloud free, cloud interstitial and residual particles.

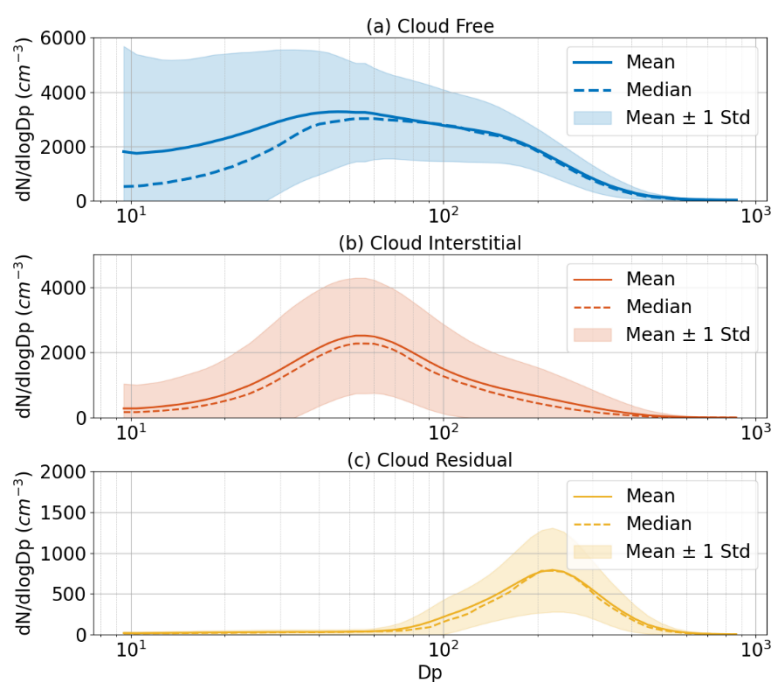


Fig. S4 The mean and median PNSD and its deviations for cloud free, cloud interstitial and residual particles.

### Back-trajectory calculation

To elucidate the air masses origin during the cloud formation under polluted conditions, the 72-hour backward trajectories arriving at Mt. Daming site were calculated for a cloud process on May 8, terminating at the height of 2000 m above ground level. The back-trajectories are calculated by applying the HYSPLIT 4 model (Hybrid Single Particle Lagrangian Integrated Trajectory) and using the NCEP GDAS (Global Data Assimilation System) data with a spatial resolution of  $1^\circ \times 1^\circ$  (Draxler and Hess, 1998).

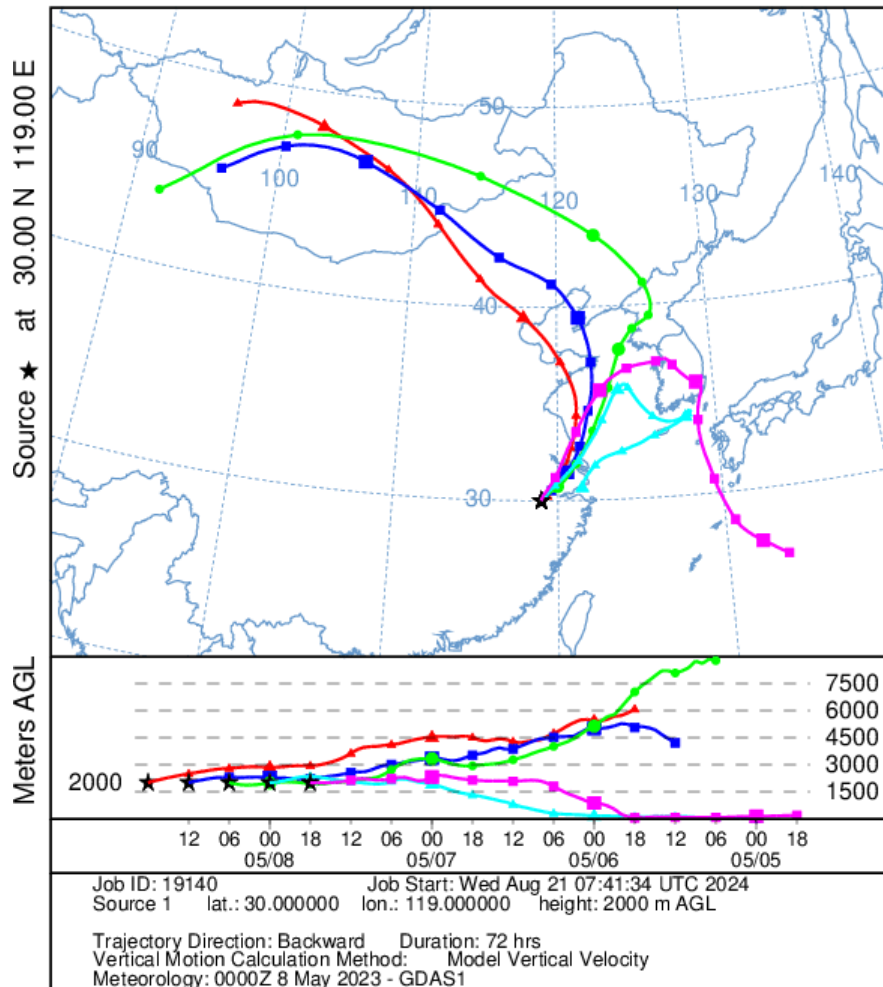


Fig. S5 The back trajectories arriving at Mt. Daming on May 8<sup>th</sup>, with the terminal height of 2000 m above ground level.

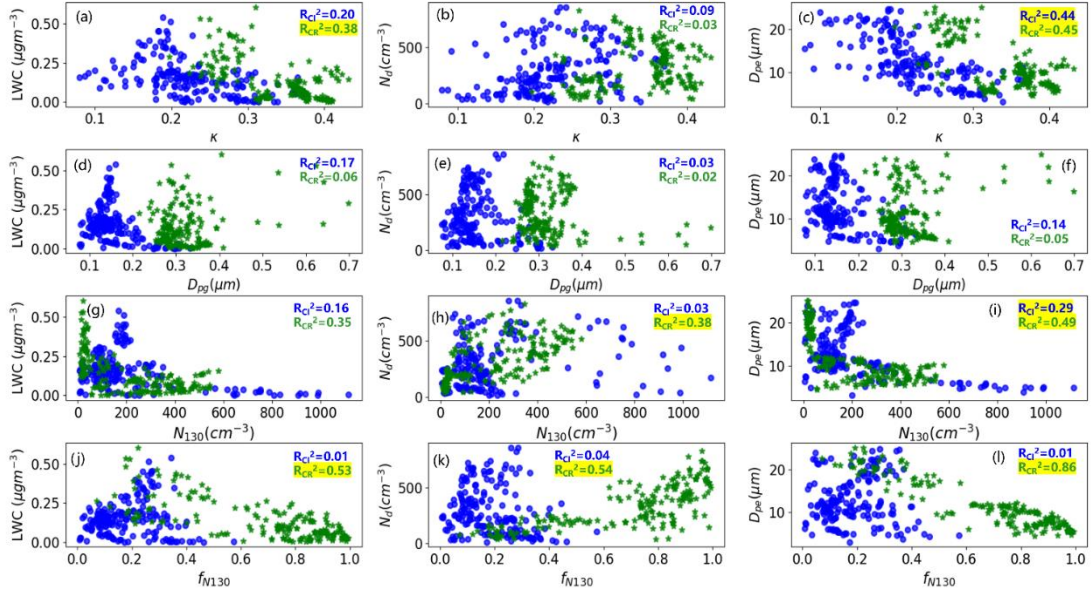


Fig. S6 Scatter plot of cloud droplet parameters (LWC,  $N_d$ , and  $D_{pe}$ ) and particle hygroscopic parameter ( $\kappa$ , a-c), geometric mean diameter ( $D_{pg}$ , d-f), number concentration above 130 nm ( $N_{130}$ , g-i) and the fraction of  $N_{130}$  accounting for total submicron particles ( $f_{N130}$ , j-l) for cloud interstitial (CI, blue circle) and residual (CR, green star) conditions, respectively. The values of  $R^2$  above 0.36 (indicating moderate and strong correlation) are highlighted by yellow.

Table S1. Key parameters including the duration time, number concentration of cloud droplet ( $N_d$ ), liquid water content ( $\text{g m}^{-3}$ ), effective diameter ( $D_{pe}$ ), activated diameter ( $D_c$ ), hygroscopicity parameter ( $\kappa$ ) and mass concentration for cloud free, cloud interstitial and residual particles

Cloud episode	$N_d$ ( $\text{cm}^{-3}$ )	LWC ( $\text{g m}^{-3}$ )	$D_{pe}$ ( $\mu\text{m}$ )	$D_c$ (nm)	$\kappa$			Mass concentration ( $\mu\text{g m}^{-3}$ )		
					CF	CI	CR	CF*	CI	CR
April 19 16:30-23:00	629±304	0.24±0.08	11.7±2.6	325	0.27±0.01	0.23±0.06	0.34±0.04	10.6±1.2	7.3±4.3	6.5±2.5
April 28 12:10-23:00	388±107	0.25±0.06	12.9±1.5	159	0.30±0.01	0.25±0.03	0.29±0.02	9.8±0.6	1.4±1.2	1.6±0.5
May 5 18:50-May 6 04:00	-	-	-	133	0.28±0.01	0.27±0.02	0.30±0.03	5.3±0.1	2.5±1.6	2.3±1.2
May 8 19:10-22:00	771±263	0.04±0.02	5.5±0.5	199	0.29±0.01	0.26±0.03	0.32±0.01	17.6±0.5	10.9±7.9	15.5±1.8

CF, CI and CR indicates the cloud free, cloud interstitial and cloud residual particles

\*The mean and standard deviation was calculated for the 30 min before cloud presence as cloud free particles

-indicates the data are not available

## References

- Draxler, R. R., and Hess, G. D.: An overview of the HYSPLIT\_4 modelling system of trajectories, dispersion, and deposition, *Aust. Meteor. Mag.*, 47, 295-308, 1998.
- Wiedensohler, A., Birmili, W., Nowak, A., Sonntag, A., Weinhold, K., Merkel, M., Wehner, B., Tuch, T., Pfeifer, S., Fiebig, M., Fjåraa, A. M., Asmi, E., Sellegri, K., Depuy, R., Venzac, H., Villani, P., Laj, P., Aalto, P., Ogren, J. A., Swietlicki, E., Williams, P., Roldin, P., Quincey, P., Hüglin, C., Fierz-Schmidhauser, R., Gysel, M., Weingartner, E., Riccobono, F., Santos, S., Grüning, C., Faloon, K., Beddows, D., Harrison, R., Monahan, C., Jennings, S. G., O'Dowd, C. D., Marinoni, A., Horn, H.-G., Keck, L., Jiang, J., Scheckman, J., McMurry, P. H., Deng, Z., Zhao, C. S., Moerman, M., Henzing, B., de Leeuw, G., Löschau, G., and Bastian, S.: Mobility particle size spectrometers: harmonization of technical standards and data structure to facilitate high quality long-term observations of atmospheric particle number size distributions, *Atmos. Meas. Tech.*, 5, 657 – 685, <https://doi.org/10.5194/amt-5-657-2012>, 2012.